



**UNIVERSITI PUTRA MALAYSIA**

**MICROWAVE-ASSISTED SYNTHESIS OF  
LAYERED DOUBLE HYDROXIDES AND  
THEIR NANOCOMPOSITES**

**OW WEE SHING TAT**

**FSAS 1999 19**

MICROWAVE-ASSISTED SYNTHESIS OF  
LAYERED DOUBLE HYDROXIDES AND  
THEIR NANOCOMPOSITES

OW WEE SHING TAT

MASTER OF SCIENCE  
UNIVERSITI PUTRA MALAYSIA

1999



**MICROWAVE-ASSISTED SYNTHESIS OF  
LAYERED DOUBLE HYDROXIDES AND  
THEIR NANOCOMPOSITES**

**By**

**OW WEE SHING TAT**

**Thesis Submitted in Fulfilment of the Requirement for the  
Degree of Master of Science in the  
Faculty of Science and Environmental Studies  
Universiti Putra Malaysia**

**August 1999**



## ACKNOWLEDGEMENTS

The author would like to take this opportunity to thank those who helped him to finish his project especially his supervisor, Associate Professor Dr Mohd Zobir Hussein and co-supervisors Associate Professor Dr Zulkarnain Zainal and Dr. Taufiq Yap Yun Hin for their guidance, advise and unlimited help

He also will like to thank the laboratory officers Mdm. Choo (ICP-AES), Puan Surina (FTIR), Encik Wahab (FTIR), Encik Zainal (FTIR), Encik Jegan (apparatus), Encik Nazri (chemical), Encik Kamal (TGA), Puan Azilah (SEM), Puan Aminah (SEM), Mr. Ho (SEM), Puan Zurina (XRD, UM), Encik Mohd. Aruf (XRD, UM), Encik Azhar (XRD, UKM), Encik Abd. Aziz (XRD, UKM) and Encik Bakar (CHNS, UKM) for their willingness to help in obtaining the spectra of the respective samples.

Beside that, he would also like to thank his family members, Associate Professor Dr. Karen Badri, Professor Dr. Badri Muhammad and his good friends (Yui, Saiful and Sharizan) for their moral support, joy and laughter.

Finally and not forgotten, Professor Dr. Hamzah Mohamad (UKM) and Dr Siti Meriam Abd. Gan (UM) for their advice on XRD works. A research fund supported by the Ministry of Science, Technology and Environment, Malaysia (MOSTE) under IRPA grant no 09-02-04-0027.

Thank!

## TABLE OF CONTENTS

	Page
ACKNOWLEDGEMENTS .....	ii
LIST OF TABLES .....	vi
LIST OF FIGURES .....	viii
LIST OF PLATES .....	xiii
LIST OF ABBREVIATIONS .....	xiv
ABSTRACT .....	xv
ABSTRAK .....	xvii
 <b>CHAPTER</b>	
<b>I INTRODUCTION.....</b>	<b>1</b>
History of Hydrotalcite .....	1
Brucite Structure .....	3
Basic Principle of Bragg's Law .....	6
Hydrotalcite Structure .....	11
Intercalation of Other Anions .....	14
Microwave Irradiation .....	17
Crystallinity .....	22
BET (Brenauer, Emmett and Teller) Surface Area Measurement.....	25
BJH (Barrett, Johner and Halenda) Pore size Distribution .....	27
Solid State Colour Analysis .....	31
 <b>II METHODOLOGY.....</b>	 <b>34</b>
Preparation of Synthetic Hydrotalcite Compounds .....	34
Materials .....	34
Method .....	34
Microwave-Assisted Synthesis of Synthetic Hydrotalcite .....	36
Materials.....	36
Method .....	36
Intercalation of Anthraquinone-2,6-Disulfonate Ion (AQ26) into Layered Double Hydroxides (Mg/Al and Zn/Al).....	37
Materials .....	37
Method .....	38
Powder X-Ray Diffraction (PXRD) Analysis .....	39
Inducted Couple Plasma – Atomic Emission Spectrometer (ICP-AES) .....	40
Chemicals .....	40
Method .....	40
Fourier Transform Infra-Red (FTIR) .....	41
Thermogravimetric Analysis (TGA) .....	41
Scanning Electron Micrograph (SEM) .....	41
Surface Area and Porosity Analyses (ASAP).....	42
Solid State Colour Analysis .....	42
 <b>III RESULTS AND DISCUSSION I: PHYSICO-CHEMICAL PROPERTIES OF HYDROTALCITE COMPOUNDS .....</b>	 <b>43</b>
Chemical Analysis .....	43
Structural Aspects .....	46
Infrared Studies of Hydrotalcite (400-4000 cm <sup>-1</sup> ).....	53
Physical Properties of Hydrotalcite .....	59



<b>IV</b>	<b>RESULTS AND DISCUSSION II: PROPERTIES OF SYNTHETIC HYDROTALCITE SYNTHESISED BY USING MICROWAVE-ASSISTED METHOD.....</b>	<b>63</b>
	Chemical Properties of HT Synthesised by Using Microwave- Assisted Method .....	63
	Microwave Effect on Crystal Formation .....	67
	Infrared Spectroscopic Studies.....	75
	Microwave Effect on Surface Area and Porosity .....	76
<b>V</b>	<b>RESULTS AND DISCUSSION III: INTERCALATION OF ANTHRAQUINONE-2,6-DISULFONATE ION INTO Mg/Al AND Zn/Al LAYERED DOUBLE HYDROXIDES BY MICROWAVE-ASSISTED METHOD .....</b>	<b>83</b>
	Chemical Analysis .....	85
	Structural Aspects .....	86
	Infrared Studies of the Intercalated AQ26 LDH .....	97
	Solid State Colour Analysis .....	105
	Composition of AQ26 and Hydrated Water for Selected Intercalated Compounds .....	109
	Physical Properties.....	113
<b>VI</b>	<b>CONCLUSIONS .....</b>	<b>118</b>
	<b>REFERENCES .....</b>	<b>121</b>
<b>APPENDIX</b>		
<b>A</b>	Crystal Radii of Some Selected Ions (pm) .....	126
<b>B</b>	JCPDS (Joint Committee on Powder Diffraction Standards) Patterns for Hydrotalcite (22-700), Brucite (7-239) and Gibbsite (12-460).....	127
<b>C1</b>	PXRD Data for (003), (006), (009), (012) and (015) Phase .....	130
<b>C2</b>	Grain Size and Crystal Strain Calculated from (003) and (006) Phase .....	131
<b>D1</b>	N <sub>2</sub> Adsorption-Desorption Isotherms for HT Synthesised by Using Conventional Method .....	135
<b>D2</b>	N <sub>2</sub> Adsorption-Desorption Isotherms for HT (R <sub>dis</sub> = 3) Synthesised by Using Microwave-Assisted Method.....	137
<b>D3</b>	N <sub>2</sub> Adsorption-Desorption Isotherms for HT (R <sub>dis</sub> = 4) Synthesised by Using Microwave-Assisted Method.....	138
<b>D4</b>	N <sub>2</sub> Adsorption-Desorption Isotherms for HT (R <sub>dis</sub> = 6) Synthesised by Using Microwave-Assisted Method .....	139
<b>D5</b>	N <sub>2</sub> Adsorption-Desorption Isotherms for Mg-Al-AQ26 Synthesised by Using Conventional (con.) and Microwave- Assisted (mic.) Methods .....	140
<b>D6</b>	N <sub>2</sub> Adsorption-Desorption Isotherms for Zn-Al-AQ26 Synthesised by Using Conventional (con.) and Microwave-Assisted (mic.) Methods.....	141
<b>E1</b>	N <sub>2</sub> /BJH Desorption Pore Size Distribution for HT Synthesised by Using Conventional Method .....	142
<b>E2</b>	N <sub>2</sub> /BJH Desorption Pore Size Distribution for HT (R <sub>dis</sub> = 3) Synthesised by Using Microwave-Assisted Method .....	144
<b>E3</b>	N <sub>2</sub> /BJH Desorption Pore Size Distribution for HT (R <sub>dis</sub> = 4) Synthesised by Using Microwave-Assisted Method .....	145

<b>E4</b>	N <sub>2</sub> /BJH Desorption Pore Size Distribution for HT ( $R_{dis} = 6$ ) Synthesised by Using Microwave-Assisted Method .....	146
<b>E5</b>	N <sub>2</sub> /BJH Desorption Pore Size Distribution for Mg–Al–AQ26 Synthesised by Using Conventional (con.) and Microwave- Assisted (mic.) Methods.....	147
<b>E6</b>	N <sub>2</sub> /BJH Desorption Pore Size Distribution for Zn–Al–AQ26 Synthesised by Using Conventional (con.) and Microwave- Assisted (mic.) Methods .....	148
<b>E7</b>	Calculation of Pore Size Distribution by Using BJH (Barrett, Johner and Halenda) Method for 1g of Sample .....	149
<b>F1</b>	BET Surface Area and Average Pore Size for HT .....	150
<b>F2</b>	BET Surface Area and Average Pore Size for Selected Intercalated Compounds .....	151
<b>G1</b>	Metals Ion Contents Using Inducted Couple Plasma – Atomic Emission Spectroscopy (ICP–AES) .....	152
<b>G2</b>	Anthraquinone-2,6-Disulfonate Content in Selected Intercalated Compounds Using CHNS and TGA .....	158
<b>H1</b>	Colour Indexes for Hydortalcite-Like Compounds with Mg–Al –AQ26 (Anthraquinone-2,6-Disulfonate) .....	159
<b>H2</b>	Colour Indexes for Hydortalcite-Like Compounds with Zn–Al –AQ26 (Anthraquinone-2,6-Disulfonate) .....	160
<b>I</b>	Character Table for $O_h$ , $D_{3d}$ , $D_{3h}$ and $C_{2v}$ Symmetries.....	161
<b>J</b>	The Electromagnetic Spectrum and Corresponding Spectroscopic Techniques .....	165
<b>VITA</b>	.....	166



## LIST OF TABLES

Table		Page
1 1	Limiting Radius for Different Coordination Numbers	3
1 2	Comparison of Some Physical and Crystallographic Parameters of <i>Pyroaurite</i> and <i>Sjögrenite</i> and Hydrotalcite.	12
1 3	Basal Spacing $d(003)$ and the Width of the 003 Reflection for Hydrotalcite-Like Compounds with Different Anions Intercalated.	15
3.1	Superlattice Cell Parameter ( $a$ ), Brucite-Like Layer Thickness ( $D$ ) and Interlayer Spacing ( $d_o \sin \alpha$ ) for HT.	48
3 2	Assignment for Free $\text{CO}_3^{2-}$ Ion in $D_{3h}$ Symmetry.	54
3 3	Normal Modes of the $\text{CO}_3^{2-}$ Ion.	55
3 4	Assignment for $\text{CO}_3^{2-}$ Ion in $C_{2v}$ Symmetry.	55
3.5	Assignment for M-O Vibration in $O_h$ Symmetry.	57
3 6	Assignment for M-O Vibration in $D_{3d}$ Symmetry.	58
3 7	Comparison of Some Surface Area Values from Miyata's Work.	59
4.1	Ratio of $\text{Al}^{3+}$ Cations ( $x$ ) in the Synthetic Hydrotalcite, Synthesised by Using Different Microwave Irradiation Times.	63
4.2	BET Surface Area Determined by Adsorption of $\text{N}_2$ on Synthetic Hydrotalcite Synthesised by Using Microwave-Assisted Method.	77
5 1	Composition of M(II) and $\text{Al}^{3+}$ in the LDH Intercalated Compounds with Anthraquinone-2,6-Disulfonate (AQ26) by Using Conventional Method.	85
5 2	Composition of M(II) and $\text{Al}^{3+}$ in the LDH Intercalated Compounds with Anthraquinone-2,6-Disulfonate (AQ26) by Using Microwave-Assisted Method.	86
5.3	Summarised of Experimental Results in the Mg/Al and Zn/Al Systems of the AQ26 Intercalated HT-Like Compounds.	90
5 4	The Calculated Slant Angle ( $\alpha$ ) of Different AQ26 Ratios for Mg/Al And Zn/Al Systems, where the $D = 4.77 \text{ \AA}$ and $d_{\text{AQ26}} = 14.3 \text{ \AA}$	93
5.5	Colour Analysis Data for Mg/Al and Zn/Al Systems Synthesised by Using Conventional Method.	105
5 6	Colour Analysis Data for Mg/Al and Zn/Al Systems Synthesised by Using Microwave-Assisted Method.	107

5.7	Percentage of Metal Ion, AQ26 and Hydrated Water in Selected Intercalated Compounds.	111
5.8	BET/N <sub>2</sub> Surface Area and BJH Desorption Average Pore Diameter for Selected Intercalated Compounds.	113



## LIST OF FIGURES

Figure		Page
1.1	Structure of hydrotalcite as suggested by Feitknecht in 1942.	1
1.2	Stacking sequences of rhombohedral symmetry ( <i>pyroaurite</i> ) and hexagonal symmetry ( <i>sjögrenite</i> ).	2
1.3	Octahedron showing octahedral coordination of six anions around a central cation for (a) NaCl and (b) Mg(OH) <sub>2</sub> where 'a' is hexagonal cell parameter.	3
1.4	Top view for brucite closed-packed structure where one layer of octahedral holes had been fully filled by metal ions (•) and the other layer is empty.	4
1.5	Side view for brucite structure where one layer of octahedral holes had been fully filled by metal ions and the other layer is empty.	5
1.6	Bragg's Law for destructive (a) and constructive (b) interference for two diffracted X-ray from different layers, where constructive interference will give signal to X-ray diffractogram.	6
1.7	Diagram shows the top view for one unit hexagonal cell of brucite sheet, where 'a' is unit cell parameter for the hexagonal cell (where '*' represents bottom layer of OH <sup>-</sup> ). $a = \sqrt{2} (r_{Mg(+2)} + r_{OH(-1)})$ .	7
1.8	Diagram shows the side view for one unit hexagonal cell of brucite sheet, where 'L' is distance between two OH <sup>-</sup> layers (where '*' represents bottom layer of OH <sup>-</sup> ). $L = \sqrt{2/3} a$ and $d(001) = D = L + 2r_{OH(-1)}$ .	8
1.9	Diagram shows the top view for brucite sheet, where 'a <sub>0</sub> ' is the distance between two metal ions in the hexagonal cell. In this case $a = a_0 = 2d(110)$ .	9
1.10	Diagram shows how OH <sup>-</sup> is tied to the CO <sub>3</sub> <sup>2-</sup> groups with two possible pathways. (a) Direct interaction, OH-CO <sub>3</sub> -HO. (b) Indirect interaction, OH-CO <sub>3</sub> -H <sub>2</sub> O-HO.	10
1.11	Joint Committee on Powder Diffraction Standards pattern for Hydrotalcite (JCPDS no. 22-700).	13
1.12	Basic design of a rectangular cavity for an EPR spectrometer.	18
1.13	Heating patterns in conventional and microwave oven.	19
1.14	Interaction of microwave with materials.	20
1.15	Gauchy profile to calculate the true half-maximum breadth, $\beta = B - \hat{b}$ .	23

1.16	Diagram of half-maximum breadth ( $B$ ), diffraction angle ( $\theta_{hkl}$ ) and broad of the peak ( $\theta_{hkl(1)}$ and $\theta_{hkl(2)}$ ) from PXRD pattern.	24
1.17	Expansion of core during desorption or vaporization of adsorbate layer.	27
1.18	BJH (Barrett, Johner and Halenda) pore size distribution form Appendix E7	31
2.1	Preparation diagram of synthetic hydrocalcite using conventional coprecipitation method in supersaturated solution for $R_{dis} = 1$ .	35
2.2	Synthesis diagram of Zn-Al-AQ26 system with 4:1:1:00 ratio	37
3.1	Ratio of $R_{from}$ and ' $x$ ' formed in HT with different ratio of $R_{dis}$ .	44
3.2	PXRD patterns for HT synthesised at different ratios of $R_{dis}$ . $R_{dis} = 2$ to 4 shows the pure phase of HT while $R_{dis} = 1$ indicate mixed phase of HT and gibbsite ( $\square$ ). $R_{dis} > 5$ indicate the formation of brucite (*).	45
3.3	Basal spacing ( $d_{003}$ ) and intensity ( $I_0$ ) for (003) phase for different ratio of $Al^{3+}$ in HT.	46
3.4	Plot of superlattice cell parameter, ' $a$ ' against ratio of $Al^{3+}$ ( $x$ ) in HT.	47
3.5	Possible orientation of carbonate ions ( $CO_3^{2-}$ ) and its effect on the values of $d(003)$ , where (a) high $Al^{3+}$ contents, (b) medium $Al^{3+}$ contents and (c) low $Al^{3+}$ contents. $d_M < d_L < d_H$ .	49
3.6	Possible distributions of $Al^{3+}$ ions (solid circles) and $Mg^{2+}$ ions (open circles) in octahedral layer structure.	50
3.7	Relative PXRD pattern intensity for $d_{015}$ and $d_{009+012}$ against the ratio of $Al^{3+}$ ( $x$ ) in HT.	51
3.8	FTIR	52
3.9	Shifting of $\nu[O-H]$ and $\delta[O-H]$ adsorption bands for HT with different ratios of $Al^{3+}$ ( $x$ ).	53
3.10	Construction of degenerate component displacements for $E'$ of $D_{3h}$ symmetry.	54
3.11	Peak shifting and peak area of $\nu_3[C-O]$ absorption band in FTIR HT with different ratios of $Al^{3+}$ ( $x$ ).	56
3.12	BET/ $N_2$ surface area and BJH desorption pore diameter for HT with different ratio of $Al^{3+}$ ( $x$ ).	59
3.13	Graph shows grain size and crystal strain against ratio of $Al^{3+}$ contents ( $x$ ) in HT.	60
4.1	PXRD patterns for HT synthesised by using microwave-assisted method at different exposure times for $R_{dis} = 3$ .	64

4.2	PXRD patterns for HT synthesised by using microwave-assisted method at different exposure times for $R_{dis} = 4$ .	65
4.3	PXRD patterns for HT synthesised by using microwave-assisted method at different exposure times for $R_{dis} = 6$ .	66
4.4	Basal spacmg of (003) reflection for the synthetic hydrotalcite synthesised by using different microwave irradiation times.	67
4.5	(003) reflection peak Intensity for the synthetic hydrotalcite synthesised by usmg different microwave irradiation times.	68
4.6	Plot of gram size calculated usmg Williamson & Hall equation of the (003) reflection peak against exposure times of microwave irradiation.	69
4.7	Graph shows crystal stram calculated using Williamson & Hall equation on the (003) reflection peak against microwave exposure times.	69
4.8	Plot of gram size calculated usmg Scherrer equation of the (003) reflection peak against exposure times of microwave irradiation.	70
4.9	Schematic diagram showing the crystal formation during microwave irradiation.	71
4.10	FTIR spectra for HT synthesised by usmg microwave-assisted method at different exposure times for $R_{dis} = 3$ .	72
4.11	FTIR spectra for HT synthesised by using microwave-assisted method at different exposure times for $R_{dis} = 4$ .	73
4.12	FTIR spectra for HT synthesised by usmg microwave-assisted method at different exposure times for $R_{dis} = 6$ .	74
4.13	Peak area of $\nu_3[\text{C-O}]$ FTIR absorption band for synthetic hydrotalcite at different microwave irradiation times.	75
4.14	Plot of peak area of $\nu_3[\text{C-O}]$ FTIR absorption band agamst grain size calculated by usmg Williamson and Hall equatron on (003) reflection peak for synthetic hydrotalcite synthesised by using microwave-assisted method.	76
4.15	Plot of BET/ $\text{N}_2$ surface area for synthetic hydrotalcite synthesised by microwave-assisted method at different irradiation times.	77
4.16	Plot of BJH desorption average pore diameter for synthetic hydrotalcite synthesised at different microwave irradiation times.	78
4.17	Plot of BJH desorption average pore diameter agamst grain size calculated by using Williamson and Hall equation on (003) reflection peak for synthetic hydrotalcite synthesised by usmg microwave-assisted method	79

5.1	PXRD patterns for the unsuccessful intercalation of organic compounds in the LDH interlayer.	84
5.2	PXRD patterns for selected intercalate compounds for Mg–Al–AQ26 and Zn–Al–AQ26 systems.	87
5.3	PXRD patterns for Mg–Al–AQ26 synthesised by using various concentration of AQ26.	88
5.4	PXRD patterns for Zn–Al–AQ26 synthesised by using various concentrations of AQ26.	89
5.5	Basal spacing for d(003) phase for Mg–Al–AQ26 and Zn–Al–AQ26 synthesised by using conventional method with different AQ26 ratios (4:1:AQ26)	91
5.6	Insulation of the orientation of Anthraquinone-2,6-disulfonate anions in the LDH.	92
5.7	PXRD patterns for Mg–Al–AQ26 with constant ratio of 4:1:0.25 synthesised at different microwave irradiation time.	94
5.8	PXRD patterns for Zn–Al–AQ26 with constant ratio of 4:1:1.00 synthesised at different microwave irradiation time.	95
5.9	d(003) for Mg–Al–AQ26 and Zn–Al–AQ26 synthesised by using microwave-assisted method at different irradiation time.	96
5.10	Intensity of (003) phase for Zn–Al–AQ26 synthesised by using microwave-assisted method at different irradiation time.	96
5.11	FTIR spectra for selected intercalate compounds for Mg/Al and Zn/Al systems.	98
5.12	FTIR spectra for Mg–Al–AQ26 synthesised by using various concentrations of AQ26.	99
5.13	FTIR spectra for Zn–Al–AQ26 synthesised by using various concentration of AQ26.	100
5.14	FTIR spectra for Mg–Al–AQ26 with constant ratio of 4:1:0.25 synthesised at different microwave irradiation time.	102
5.15	FTIR spectra for Zn–Al–AQ26 with constant ratio of 4:1:1.00 synthesised at different microwave irradiation time.	103
5.16	Peak area for asym $\nu$ [S–O] absorption band in FTIR spectra for Mg–Al–AQ26 and Zn–Al–AQ26 synthesised by using conventional method with different AQ26 ratios (4:1:AQ26).	104
5.17	Peak area for asym $\nu$ [S–O] absorption band in FTIR spectra for Mg–Al–AQ26 and Zn–Al–AQ26 synthesised by using microwave-assisted method at different irradiation time.	104

5.18	Colour difference ( $\Delta E^*_{ab}$ ) for Mg–Al–AQ26 and Zn–Al–AQ26 synthesised by using conventional method with different AQ26 ratios (4:1:AQ26).	106
5.19	Chrominance difference ( $\Delta C^*_{ab}$ ) for Mg–Al–AQ26 and Zn–Al–AQ26 synthesised by using conventional method with different AQ26 ratios (4:1:AQ26).	106
5.20	Hue difference ( $\Delta H^*_{ab}$ ) for Mg–Al–AQ26 and Zn–Al–AQ26 synthesised by using conventional method with different AQ26 ratios (4:1:AQ26).	108
5.21	Colour difference ( $\Delta E^*_{ab}$ ) for Mg–Al–AQ26 and Zn–Al–AQ26 synthesised by using microwave-assisted method with different irradiation time.	108
5.22	Chrominance difference ( $\Delta C^*_{ab}$ ) for Mg–Al–AQ26 and Zn–Al–AQ26 synthesised by using microwave-assisted method with different irradiation time.	109
5.23	Hue difference ( $\Delta H^*_{ab}$ ) for Mg–Al–AQ26 and Zn–Al–AQ26 synthesised by using microwave-assisted method with different irradiation time.	110
5.24	Types of Anthraquinone-2,6-disulfonate acid and ions, which can exist in the intercalated compounds.	112

## LIST OF PLATES

Plate		Page
1.1	Microwave Digestion System (MDS-2100). On the right is high performance vessel.	39
3.1	Scanning Electrons Micrographs (SEM) for HT at 2000 X magnification.	61
4.1	SEM surface morphology of the synthetic hydrotalcite synthesised by using microwave-assisted method at different microwave irradiation times.	80
5.1	Scanning Electrons Micrographs (SEM) of selected intercalated compounds.	114



## LIST OF ABBREVIATIONS

AQ26	Anthraquinone-2,6-disulfonate anion
ASAP	Analysis Surface Area and Porosity
BET	Brenauer, Emmett and Teller
BJH	Barrett, Johner and Halenda
CHNS	Carbon, Hydrogen, Nitrogen Analysis
D	Brucite-like layer thickness
DCIE	Different Colour Index Evaluation
$D_{avg}^p$	Average pore diameter
FTIR	Fourier Transform Infra-red
HT	Hydrotalcite
ICP-AES	Inductived Couple Plasma – Atomic Emission Spectroscopy
JCPDS	Joint Committee on Powder Diffraction Standards
LDH	Layered Double Hydroxide
M(II)	Divalent metal ions, $Mg^{2+}$ or $Zn^{2+}$
$P_r$	Relative pressure
PXRD	Powder X-ray Diffraction
$R_{dis}$	Ratio of $Mg^{2+}$ to $Al^{3+}$ discharged, $R = Mg/Al$
$R_{form}$	Ratio of $Mg^{2+}$ to $Al^{3+}$ formed
$r^c$	Core radius
$r^p$	Pore radius
SEM	Scanning Electron Microscopy / Micrograph
$\tau$	Adsorbate layer thickness
TGA	Termogravimetric Analysis
$a$	Superlattice cell parameter for hexagonal
$x$	Fraction of $Al^{3+}$ in brucite-like layer, $x = Al/(Al+Mg)$
$\alpha$	Slant angle
$\beta$	True half-maximum breadth
$\theta$	X-ray diffraction angle
$\delta A^p$	Incremental surface area
$\delta v^p$	Incremental pore volume
$\eta$	Crystal strain



Abstract of thesis presented to the Senate of Universiti Putra Malaysia in fulfilment of the requirements for the degree Master of Science

**MICROWAVE-ASSISTED SYNTHESIS OF  
LAYERED DOUBLE HYDROXIDES AND  
THEIR NANOCOMPOSITES**

By

**OW WEE SHING TAT**

August 1999

**Chairman: Associate Professor Mohd. Zobir Hussein, Ph.D.**

**Faculty: Science and Environmental Studies**

A series of hydrotalcite (HT) compounds of the type  $[Mg_{1-x}Al_x(OH)_2][CO_3]_{x/2} \cdot nH_2O$  had been synthesised using conventional co-precipitation method with  $R_{dis} = Mg/Al = 1$  to 10 in order to establish the relationship between composition and the basic properties. It was found that pure HT compounds were obtained in the range of  $R_{dis} = 2$  to 4. The materials were also synthesised by microwave-assisted method using a home cooking microwave oven at various ageing times, from 0.5 to 10.0 minutes. The discharge ratio of  $R_{dis} = 3, 4,$  and 6 were chosen in this study. The resulting synthetic materials afford well-crystallised hydrotalcite even at a very short microwave exposure time of about 60 minutes as compared with the conventional method that took about 18hrs. However, the conventional method gave good crystallinity. On the other hand, the microwave-assisted method gave better pore size distribution as compared to the conventional method. Better crystallinity was observed as the exposure time increased for all  $R_{dis}$ . Structural characterisations were done by powder X-ray diffraction (PXRD). The grain sizes and crystal strain of the materials using PXRD were calculated.

Modification of hydrotalcite had also been done by replacing its anions with anthraquinone-2,6-disulfonate ions (AQ26), which were present in the interlayer of brucite-like  $([Mg_{1-x}Al_x(OH)_2]^{x+}$  and  $[Zn_{1-x}Al_x(OH)_2]^{x+}$ ). Layered nanocomposite materials were prepared by using direct synthesis method which involved adding NaOH(aq) into a mixed of



M(II)(NO<sub>3</sub>)<sub>2</sub>, Al<sub>2</sub>(NO<sub>3</sub>)<sub>3</sub> and Na<sub>2</sub>(AQ26) aqueous solutions at pH7.50 ± 0.05 with different M(II):Al:AQ26 ratios of 4:1:0.00, 4:1:0.10, 4:1:0.25, 4:1:0.50 and 4:1:1.00. The expansion of the galleries height from 8.9 Å to 19.1 Å had been observed in X-ray diffraction data that indicating that the intercalation of the AQ26 anion replacing the nitrate anion in the interlayer of the layered double hydroxide had occurred. This conclusion has been supported by the FTIR spectrum that shows the co-existence of NO<sub>3</sub><sup>-</sup> anion that gave sharp absorption band at 1380 cm<sup>-1</sup> (ν[N-O]) and broad peak at 1200 cm<sup>-1</sup> for asym ν[S-O] for AQ26. Only M(II):Al:AQ26 ratio of 4:1:0.25 and above gave pure AQ26 intercalated LDH with no presence of NO<sub>3</sub><sup>-</sup> anion in the interlayer. These ratios showed that AQ26 anion was perpendicular to the metal hydroxide layer (α = 90°). Three types of AQ26 species (i.e. AQ26<sup>2-</sup>, AQ26<sup>-</sup> and neutral) had been suspected to exist in the interlayer.

In the microwave-assisted method, the ratio of 4:1:0.25 for Mg-Al-AQ26 system and 4:1:1.00 for Zn-Al-AQ26 system had been studied because of their good crystallinity. However microwave-assisted method, the Zn-Al-AQ26 system gave negative effect with the formation of ZnO. The formation of ZnO would increase with increasing exposure time. The Mg-Al-AQ26 system of other hand, gave poor crystal formation. The BET surface area increased from 92.8 to 112.4 m<sup>2</sup>/g, showing an increase of 21% by using microwave-assisted method for Mg-Al-AQ26 system. The ratio of mother solution changed from 4:1:0.25 to 4:2.90:2.35 (conventional method) and 4:3.41:1.50 (microwave-assisted method) for Mg-Al-AQ26 system while changes from 4:1:1.00 to 4:1.02:1.67 and 4:0.97:1.63 for conventional and microwave-assisted methods respectively were observed for Zn-Al-AQ26 system.

Abstrak tesis yang dikemukakan kepada Senat Universiti Putra Malaysia sebagai memenuhi keperluan untuk ijazah Master Sains.

**SINTESIS SEBATIAN HYDROKSIDA BERLAPIS GANDA  
DAN NANOKOMPOSITNYA DENGAN  
BANTUAN GELOMBANG MIKRO**

Oleh

**OW WEE SHING TAT**

Ogos 1999

**Pengerusi: Profesor Madya Mohd. Zobir Hussein, Ph.D.**

**Fakulti: Sains dan Pengajian Alam Sekitar**

Satu siri  $R_{dis} = 1$  hingga 10 hidrotalsit (HT) jenis  $[Mg_{1-x}Al_x(OH)_2][CO_3]_{x/2}.mH_2O$  telah disintesis dengan menggunakan kaedah konvensional ko-pemendakan untuk mendapatkan perkaitan antara komposisi dan sifat-sifat umum. Didapati pada julat  $R_{dis} = 2$  hingga 4 fasa hidrotalsit tulen telah dihasilkan. Kaedah sintesis bantuan gelombang mikro dengan menggunakan ketuhar gelombang mikro biasa pada masa pendedahan dari 0.5 ke 10.0 minit dengan  $R_{dis} = 3, 4$  dan 6 dipilih untuk kajian ini. Keputusan menunjukkan pembentukan hablur yang baik berlaku pada masa yang singkat lebih kurang 6.0 minit dengan menggunakan kaedah bantuan gelombang mikro berbanding dengan kaedah konvensional yang mengambil masa lebih kurang 18 jam. Akan tetapi kaedah konvensional masih memberikan pembentukan hablur terbaik. Walaubagaimana pun, kaedah bantuan gelombang mikro memberikan taburan saiz liang yang lebih sekata jika dibanding dengan kaedah konvensional. Ia memberikan pembentukan hablur yang baik pada masa pendedahan yang lama untuk semua  $R_{dis}$ . Kajian sifat struktur sebatian menggunakan kaedah pembelauan sinar-X dalam keadaan serbuk dijalankan. Saiz dan ketegangan hablur dikira daripada data pembelauan sinar-X.

Modifikasi pada hidrotalsit dilakukan dengan menggantikan amon inter-lapisan seakan brusit ( $[Mg_{1-x}Al_x(OH)_2]$  dan  $[Zn_{1-x}Al_x(OH)_2]$ ) dengan ion antrakuinon-2,6-disulfonik. Sebatian nanokomposit berlapis disintesis dengan kaedah pemendakan terus di mana



larutan NaOH(ak) ditambahkan kedalam larutan campuran garam  $M(II)(NO_3)_2$ ,  $Al_2(NO_3)_3$  dan  $Na_2(AQ26)$  pada  $pH 7.50 \pm 0.05$  dengan nisbah  $M(II):Al: AQ26$  pada 4:1:0.00, 4:1:0.10, 4:1:0.25, 4:1:0.50 dan 4:1:1.00. Pengembangan jarak inter-lapisan daripada 8.9 Å kepada 19.1 Å dalam data pembelauan sinaran-X menunjukkan interkalasi AQ26 menggantikan anion nitrat pada inter-lapisan dalam hidroksida berlapis ganda. Kenyataan ini disokong oleh data Infra-merah yang menunjukkan kewujudan bersekali anion  $NO_3^-$  yang membenarkan serapan yang tajam pada  $1380\text{ cm}^{-1}$  ( $\nu[N-O]$ ) dan serapan lebar pada  $1200\text{ cm}^{-1}$  bagi antisym  $\nu[S-O]$  untuk AQ26. Hanya nisbah 4:1:0.25 atau lebih bagi  $M(II):Al: AQ26$  membenarkan interkalasi AQ26 tulen tanpa kewujudan anion  $NO_3^-$  pada inter-lapisan. Nisbah ini menunjukkan anion AQ26 berkedudukan tegak terhadap lapisan logam hidroksida ( $\alpha = 90^\circ$ ). Tiga jenis spesis AQ26 (iaitu  $AQ26^{2-}$ ,  $AQ26^-$  dan neutral) disyaki wujud dalam inter-lapisan.

Dalam kaedah bantuan gelombang mikro, nisbah 4:1:0.25 bagi sistem Mg–Al–AQ26 dan 4:1:1.00 bagi sistem Zn–Al–AQ26 digunakan dalam kajian kerana pembentukan hablur yang baik. Walaubagaimana pun, kaedah bantuan gelombang mikro bagi sistem Zn–Al–AQ26 menunjukkan kesan negatif dengan pembentukan ZnO. Pembentukan ZnO bertambah bila masa pendedahan bertambah. Dibalikannya, sistem Mg–Al–AQ26 memberi pembentukan hablur yang kurang baik. Luas permukaan BET bertambah sebanyak 21% daripada 92.8 kepada 112  $m^2/g$  dengan menggunakan kaedah bantuan gelombang mikro bagi sistem Mg–Al–AQ26. Nisbah larutan induk berubah daripada 4:1:0.25 kepada 4:2.90:2.35 (kaedah konvensyenal) dan 4:3.99:1.10 (kaedah bantuan gelombang mikro) bagi sistem Mg–Al–AQ26, manakala bagi sistem Zn–Al–AQ26 perubahan dari 4:1:1.00 kepada 4:1.02:1.67 dan 4:0.97:1.63.

## CHAPTER I

### INTRODUCTION

#### History of Hydrotalcite

Hydrotalcite was first discovered in Sweden around 1842 as natural mineral clay that can be easily crushed into a white powder. Later, Professor E. Manasse [1] of mineralogy at University of Florence, Italy, found that this mineral is made up of magnesium, aluminium, hydroxides, carbonate and water molecules. Its exact formula is  $Mg_6Al_2(OH)_{16}CO_3 \cdot 4H_2O$ . Due to inadequate crystallographic data led to an uncertainty of the hydrotalcite structure at that time. In 1942, Feitknecht [2] proposed that the structure of these clays consists of a double sheet structure as follows:

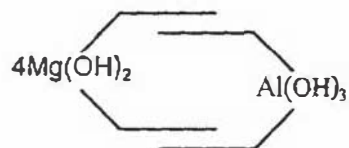


Figure 1.1: Structure of hydrotalcite as suggested by Feitknecht in 1942 [2].

Feitknecht named it “*doppelschichtstrukturen*” which mean “double sheet structure”, in which the magnesium hydroxides and aluminium hydroxides are on different sheets. From an X-ray investigation by Aminoff and Broome [3], it was shown that hydrotalcite had two polytypes, namely rhombohedral and hexagonal. The actual structure of hydrotalcite has been determined by Allmann in 1968 [4], it was composed of positively charged

brucite-like ( $\text{Mg}(\text{OH})_2$ ) layers of divalent ( $\text{Mg}^{2+}$ ) and trivalent ( $\text{Al}^{3+}$ ) metal hydroxides ( $[\text{Mg}_{1-x}\text{Al}_x(\text{OH})_2]^{x+}$ ) located in the same layer. Excess positive charge was compensated or stabilised by carbonate anions that are negatively charged with water molecules presented in the interstitial position. The rhombohedral and hexagonal structures are known as *pyroaurite* and *sjögrenite* [5], respectively.

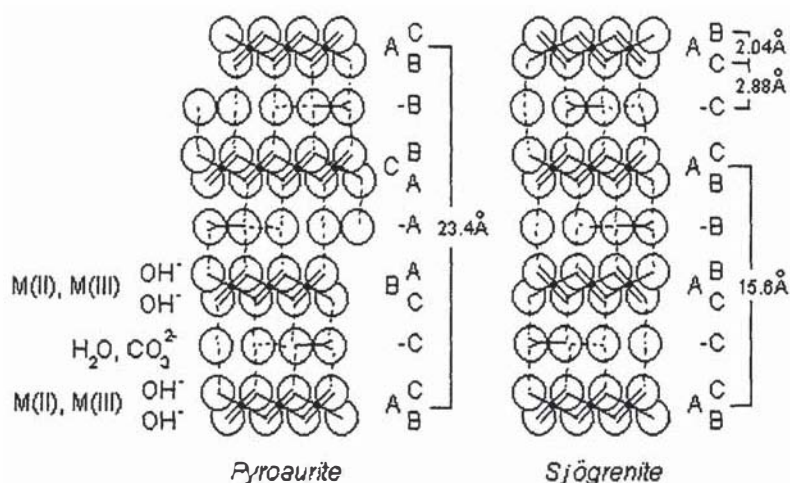


Figure 1.2: Stacking sequences of rhombohedral symmetry (*pyroaurite*) and hexagonal symmetry (*sjögrenite*) [5].

Other natural clay minerals that have shown the same structure as hydrotalcite (they so-called hydrotalcite-like compounds) have also been found such as iowaite ( $\text{Mg}^{2+}\text{-Fe}^{3+}\text{-Cl}^-$ ), meixmente ( $\text{Mg}^{2+}\text{-Al}^{3+}\text{-OH}^-$ ), carrboydite ( $\text{Ni}^{2+}\text{-Al}^{3+}\text{-SO}_4^{2-}$ ), motukorecite ( $\text{Mg}^{2+}\text{-Al}^{3+}\text{-SO}_4^{2-}$ ), honessite ( $\text{Ni}^{2+}\text{-Fe}^{3+}\text{-SO}_4^{2-}$ ) and woodwardite ( $\text{Cu}^{2+}\text{-Al}^{3+}\text{-SO}_4^{2-}$ ) [6]. The first paper in open literature referring to hydrotalcite-like compounds appeared in 1971, written by Miyata *et al.* [7] dealing with basic catalysis. Hydrotalcite was synthesised in the laboratory for the first time by Allmann [8] in 1968 by using  $\text{MgCl}_2$  and  $\text{AlCl}_3$  mixed solution titrated with  $\text{NaOH}$  and  $\text{Na}_2\text{CO}_3$  mixed solution. Later it Powder X-ray Diffraction (PXRD) data patterns were recorded in JCPDS (Joint Committee on Powder Diffraction Standards) pattern number 22-700 (Appendix B).

## Brucite Structure

The hydrotalcite structure ( $[\text{Mg}_{1-x}\text{Al}_x(\text{OH})_2]^{x+}[\text{CO}_3^{2-}]_{x/2} \cdot m\text{H}_2\text{O}$ ) is resembled of that brucite-like structure ( $\text{Mg}(\text{OH})_2$ ). The only difference is that hydrotalcite consists of a brucite-like layer structure that has anions and water molecules between the layers. In ionic (ceramic) solid, the packing of the ions is determined primarily by the following factors:

1. The relative size of the ions in the ionic solid, as shown in the table below:

Table 1.1: Limiting Radius for Different Coordination Numbers [9].

Coordination number	Geometry	Limiting radius ratio
4	Tetrahedral	0.225
6	Octahedral	0.414
8	Cubic	0.732
		1.00

2. The need to balance electrostatic charges to maintain electrical neutrality in the ionic solid.

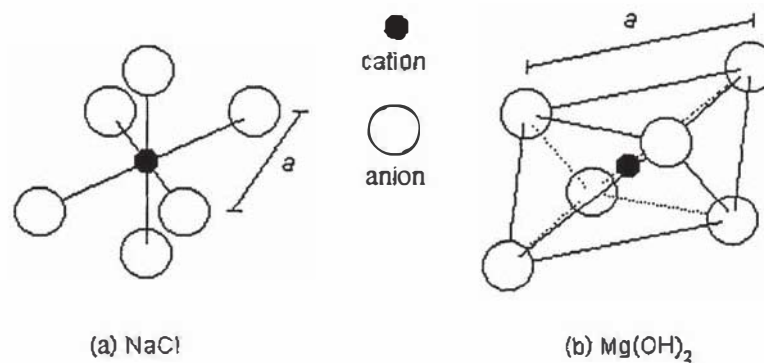


Figure 1.3: Octahedron showing octahedral coordination of six anions around a central cation for (a) NaCl and (b)  $\text{Mg}(\text{OH})_2$  where 'a' is hexagonal cell parameter.

The relative size for  $r_{\text{Mg}^{+2}}/r_{\text{OH}^{-1}} = 0.86 \text{ \AA}/1.23 \text{ \AA} = 0.70$ , and at this condition  $\text{Mg}^{2+}$  is suitable to fill in the octahedral sites where 'a' was regarded as hexagonal superlattice parameter [10], with a structure similar to NaCl (Figure 1.3) showing octahedral

coordination of  $\text{Cl}^-$  anions around a central  $\text{Na}^+$  cation where the  $r_{\text{Na}^{(+1)}}/r_{\text{Cl}^{(-1)}} = 1.16 \text{ \AA} / 1.67 \text{ \AA} = 0.70$ , which is greater than 0.414 but less than 0.732.

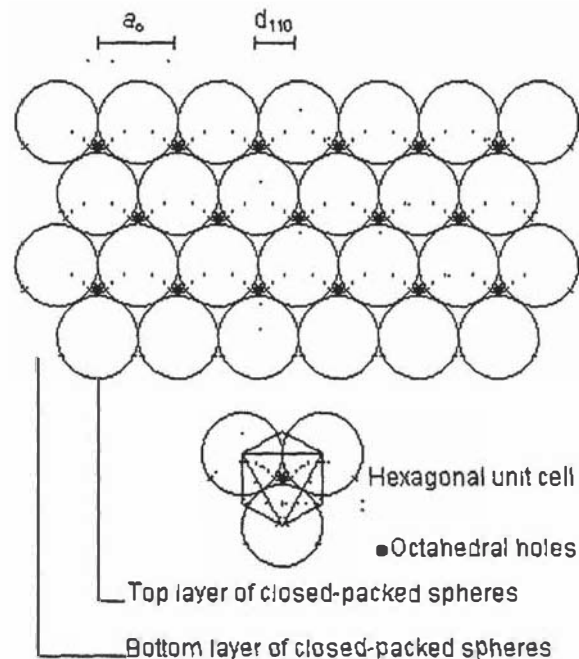


Figure 1.4: Top view for brucite closed-packed structure where one layer of octahedral holes had been fully filled by metal ions ( $\bullet$ ) and the other layer is empty.

$\text{Mg}^{2+}$  ion has two positive charges while  $\text{OH}^-$  ion has one negative charge. Therefore to stabilise the charge, one  $\text{Mg}^{2+}$  ion must be accompanied by two  $\text{OH}^-$  ions. In this case the coordination ratio of cation to anion coordination has to be 1:2. When half of the octahedral holes have been filled by cations, the coordination ratio will be 6:3. Figure 1.4 shows what the close-packed structure looks like.

Here, six oxygen atoms in the form of hydroxides octahedrally surround the magnesium cation, resulting in octahedral shared edges to form an infinite sheet. These sheets are stacked on top of each other and are held together by hydrogen bonds, as shown in Figure 1.5.

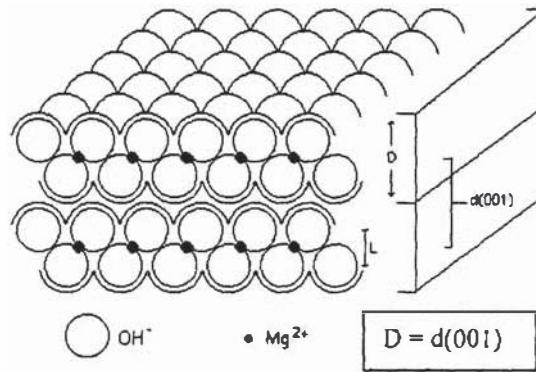


Figure 1.5: Side view for brucite structure where one layer of octahedral holes had been fully filled by metal ions and the other layer is empty.

If 'a' is parameter of the hexagonal unit cell corresponding to the distance between two metal ions in an adjacent octahedral site or hydroxide ions, the thickness of the brucite sheet can be calculated. Where distance between top and bottom hydroxide sheets is 'L'.

$$a = \sqrt{2} r_{(M-OH)} \quad [1-1]$$

$$L = (2/\sqrt{3})r_{(M-OH)} \quad [1-2]$$

where  $r_{(M-OH)}$  is the metal ion–hydroxide ion distance,

$$r_{(M-OH)} = r_{Mg(+2)} + r_{OH(-1)} \quad [1-3]$$

Therefore, the layer thickness will be 'D' (Figures 1.7 and 1.8 can be referred to verification of these equations).

$$\begin{aligned}
 D &= L + 2r_{OH(-1)} \\
 &= (2/\sqrt{3})r_{(M-OH)} + 2r_{OH(-1)}
 \end{aligned} \quad [1-4]$$